Brain Struct Funct
DOI 10.1007/s00429-016-1198-9

ORIGINAL ARTICLE

Connectivity between the central nucleus of the amygdala and the bed nucleus of the stria terminalis in the non-human primate: neuronal tract tracing and developmental neuroimaging studies

Jonathan A. Oler[1,7] · Do P. M. Tromp[1,7] · Andrew S. Fox[1,2,7] · Rothem Kovner[1,7] · Richard J. Davidson[1,2] · Andrew L. Alexander[1,3] · Daniel R. McFarlin[1,7] · Rasmus M. Birn[1,3] · Benjamin E. Berg[4] · Danielle M. deCampo[5] · Ned H. Kalin[1,2,7] · Julie L. Fudge[5,6]

Received: 6 August 2015 / Accepted: 30 January 2016

Abstract The lateral division of the bed nucleus of the stria terminalis (BSTL) and central nucleus of the amygdala (Ce) form the two poles of the 'central extended amygdala', a theorized subcortical macrostructure important in threat-related processing. Our previous work in nonhuman primates, and humans, demonstrating strong resting fMRI connectivity between the Ce and BSTL regions, provides evidence for the integrated activity of these structures. To further understand the anatomical substrates that underlie this coordinated function, and to investigate the integrity of the central extended amygdala early in life, we examined the intrinsic connectivity between the Ce and BSTL in non-human primates using ex vivo neuronal tract tracing, and in vivo diffusion-weighted imaging and resting fMRI techniques. The tracing studies revealed that BSTL receives strong input from Ce; however, the reciprocal pathway is less robust, implying that the primate Ce is a major modulator of BSTL function. The sublenticular extended amygdala (SLEAc) is strongly and reciprocally connected to both Ce and BSTL, potentially allowing the SLEAc to modulate information flow between the two structures. Longitudinal early-life structural imaging in a separate cohort of monkeys revealed that extended amygdala white matter pathways are in place as early as 3 weeks of age. Interestingly, resting functional connectivity between Ce and BSTL regions increases in coherence from 3 to 7 weeks of age. Taken together, these findings demonstrate a time period during which information flow between Ce and BSTL undergoes postnatal developmental changes likely via direct Ce → BSTL and/or Ce ↔ SLEAc ↔ BSTL projections.

Keywords Sublenticular extended amygdala · Bed nucleus of the stria terminalis · Central nucleus · Fear · Anxiety · DTI · Functional connectivity

Abbreviations

Ac	Anterior commissure
ABmc	Accessory basal nucleus, magnocellular subdivision
Astr	Amygdalostriatal transition zone
Bi	Basal nucleus, intermediate subdivision
Bmc	Basal nucleus, magnocellular subdivision
Bpc	Basal nucleus, parvicellular subdivision
BST	Bed nucleus of the stria terminalis
BSTL	Lateral bed nucleus of the stria terminalis
BSTLc	Lateral bed nucleus of the stria terminalis, capsular subdivision
BSTLcn	Lateral bed nucleus of the stria terminalis, central subdivision

J. A. Oler and D. P. M. Tromp contributed equally to this manuscript.

J. L. Fudge and N. H. Kalin share senior authorship.

✉ Jonathan A. Oler
oler@wisc.edu

[1] Department of Psychiatry, University of Wisconsin School of Medicine and Public Health, Madison, USA

[2] Department of Psychology, University of Wisconsin-Madison, Madison, USA

[3] Department of Medical Physics, University of Wisconsin School of Medicine and Public Health, Madison, USA

[4] Allegheny College, Meadville, USA

[5] Department of Neuroscience, University of Rochester Medical Center, Rochester, USA

[6] Department of Psychiatry, University of Rochester Medical Center, Rochester, USA

[7] HealthEmotions Research Institute, Wisconsin Psychiatric Institute and Clinics, 6001 Research Park Blvd., Madison, WI 53719, USA

Published online: 23 February 2016

BSTLj	Lateral bed nucleus of the stria terminalis, juxtacapsular subdivision
BSTLP	Lateral bed nucleus of the stria terminalis, posterior subdivision
C	Caudate nucleus
Ce	Central nucleus
CeLcn	Central nucleus, lateral central subdivision
CeLc	Central nucleus, lateral capsular subdivision
CeM	Central nucleus, medial subdivision
EAc	Central extended amygdala
GP	Globus pallidus
GPe	Globus pallidus, pars externa
GPi	Globus pallidus, pars interna
H	Hippocampus
Ic	Internal capsule
L	Lateral nucleus
M	Medial nucleus
NBM	Nucleus basalis of Meynert
P	Putamen
S	Shell of the ventral striatum
SLEAc	Sublenticular extended amygdala, central subdivision
ST	Stria terminalis
V	Ventricle
VA	Ventral amygdalofugal pathway
VP	Ventral pallidum

Introduction

Using a combination of imaging, tract tracing, and lesion techniques, we have focused on the roles for the amygdala and the bed nucleus of the stria terminalis (BST) in the expression of primate anxiety (deCampo and Fudge 2013; Fox and Kalin 2014). Many neuroanatomists consider the central nucleus of the amygdala (Ce), the lateral subnuclei of the BST (BSTL), and the cell columns in the basal forebrain that bridge them (the central division of the sublenticular extended amygdala, SLEAc) to be components of a 'central extended amygdala' (EAc) macrostructure (Alheid and Heimer 1988; de Olmos and Ingram 1972; Heimer et al. 1991; Johnston 1923; McDonald 2003), although this concept is not accepted by other groups (Bienkowski and Rinaman 2013; Swanson 2003; Swanson and Petrovich 1998). The EAc arises from the 'sub-pallial' ganglionic eminence in the embryo (Bupesh et al. 2011), is intimately linked to amygdala proper (Freese and Amaral 2009; Yilmazer-Hanke 2012), hypothesized to play an important role in neuropsychiatric disorders (Heimer et al. 1997) and recognized as a key site for threat-monitoring behaviors (Fox et al. 2015). Classic studies, mostly performed in rodents, define the EAc in part, by: (1) 'symmetric' organization of the BSTL and Ce subdivisions in terms of neuropeptide and transmitter markers (Alheid and Heimer 1988; McDonald 2003); (2) robust connections among the BSTL, Ce and SLEAc (Grove 1988a, b); and (3) many common afferent and efferent projections (Gray and Magnuson 1987, 1992; McDonald et al. 1999; Moga et al. 1990; Nagy and Pare 2008; Reynolds and Zahm 2005; Rinaman et al. 2000; Wallace et al. 1992). These anatomical features, together with functional imaging studies (Birn et al. 2014; Oler et al. 2012; Torrisi et al. 2015) suggest that the EAc is both a structural and functional unit. However, few anatomic data exist to validate these concepts in primates.

The amygdala is connected to the BST via two major fiber bundles (see Fig. 1), the ventral amygdalofugal pathway (VA, also called the *ansa peduncularis*) and the stria terminalis (ST) (Nauta 1961). VA fibers project through the SLEAc region of the basal forebrain, directly connecting the Ce and other amygdalar nuclei with the BST (Heimer and Van Hoesen 2006; Novotny 1977). The ST, on the other hand, exits the caudal amygdala, arching dorsally and rostrally over the thalamus carrying with it efferent fibers from Ce and other amygdalar nuclei, which terminate in the BSTL and also pass through it en route to deeper brain structures that mediate the neuroendocrine and somatomotor responses to stress (Amaral et al. 1992; Klingler and Gloor 1960).

Using fMRI, we demonstrated strong 'resting-state' functional connectivity between the Ce and the BST in both monkeys and humans (Birn et al. 2014; Oler et al. 2012), and several studies have used diffusion tensor imaging (DTI) to visualize the structural connectivity of the ST and VA fiber pathways (Avery et al. 2014; Krüger et al. 2015; Mori and Aggarwal 2014; Veraart et al. 2011). Importantly, such in vivo techniques provide the opportunity to repeatedly examine the structure and function of the EAc in living individuals over time. However, DTI does not allow for the determination of the directionality of projections, nor discrimination between passing fiber tracts and those giving rise to terminating axonal fields. Therefore, we now present data from neuronal tract tracing techniques in nonhuman primates to assess the directionality of Ce-BSTL projections, and to visualize, at a microscopic level, local circuitry within the EAc.

We also previously found that around 2 months of age, infant monkeys develop the ability to adaptively modulate their threat-related defensive behaviors, which likely involve the EAc (Kalin et al. 1991). Therefore, in the current study we used in vivo imaging to complement the tract tracing, and to characterize the structural and functional integrity of the EAc longitudinally at 3 weeks and 7 weeks of age. Together with the detailed ex vivo tract tracing studies, the developmental imaging studies provide insights into the organization of the EAc, and its ontogeny early in life.

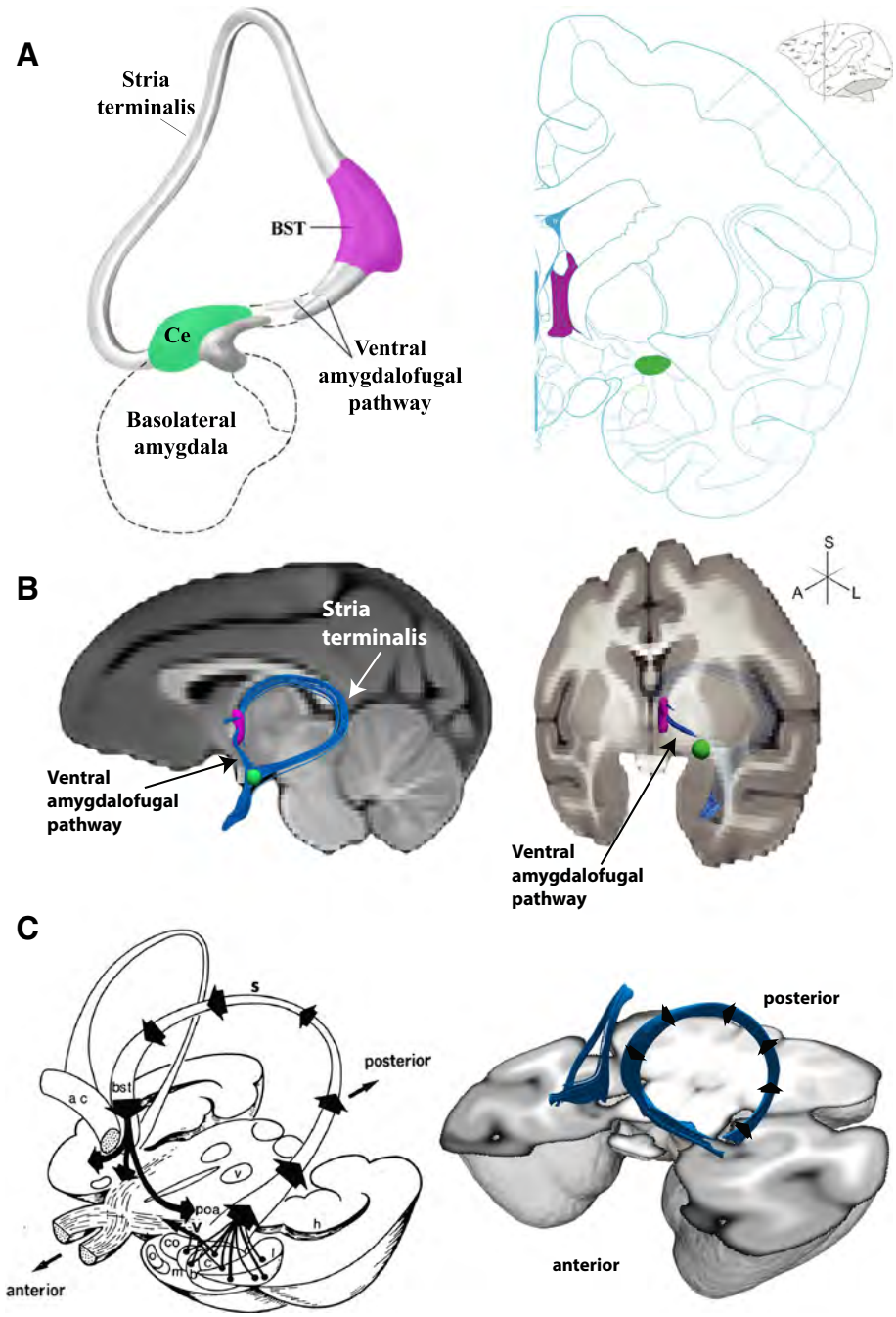

Fig. 1 The EAc and its white matter pathways. **a** *Left* a schematic of the extended amygdala concept as proposed by Heimer and colleagues (Heimer et al. 1999), and *right* a plate from a rhesus monkey brain atlas (Paxinos et al. 2009) highlighting the location of the BST (*purple*) and Ce (*green*). **b** *Left* mid-sagittal and *right* rotated coronal MRI slices through a rhesus monkey brain template with an overlaid rendering of the deterministic tractography results showing the pathways connecting the BST and Ce. Also depicted are the waypoint ROIs used in the analysis to define the BST (*purple*) and Ce (*green*). Note that the ST in the sagittal view is projected in 3D out in front of the MRI slice. The ST is occluded in the tilted coronal view, traveling caudally behind the MRI slice then arching dorsally and rostrally back out in front of the MRI slice, into the BST waypoint. **c** *Left* a classic drawing (Roberts 1992) of the major axonal pathways leaving the amygdala, and *right* a 3D tractography rendering of bilateral ST/VA pathways

Materials and materials

Imaging studies and methods

Subjects

MRI Twenty-eight preadolescent rhesus monkeys (*Macaca mulatta*, mean age; 636 days [standard deviation; 227 days], 12 females) were first used to delineate the white matter tracts connecting the Ce and BST regions. To study extended amygdala connectivity early in life, an additional six neonatal rhesus monkeys (three male and three female) were used. MRIs for the neonate cohort were acquired at two developmental time points. Mean age at first MR scan was 21 days (range 20–23 days); mean age at second MR scan was 49 days (range 48–50 days). Only 5 of the 6 baby monkeys had usable fMRI data from both time points. The monkeys were born and reared at the Wisconsin National Primate Research Center (WNPRC) and the Harlow Center for Biological Psychology. Animals

were typically pair housed in a standard primate cage; the neonates were housed with their mothers. Animals were fed twice daily and water was available ad libitum. Animal housing room lights were on a 12-h light–dark cycle.

MRI acquisition

Preadolescent cohort MRI images were acquired after the animals received ketamine 15 mg/kg and dexmedetomidine 15 μg/kg prior to scan. The animal was then placed in a stereotactic device while heart rate and oxygen saturation were monitored. Dextrose solution was administered as needed. Animals received a ketamine- 2.5 mg/kg booster before the last scan sequence, and atipamezole 150 μg/kg immediately following scan. MRI scans were obtained using a GE SIGNA 750 3.0 T scanner (General Electrics, Milwaukee, WI, USA) with a quadrature extremity radio-frequency (RF) coil in which the stereotaxic frame fit in the center of the coil.

Infant cohort For both scan acquisitions, the neonatal animals were initially anesthetized with ketamine HCL (20 mg/kg). All animals were given atropine sulfate (0.04 mg/kg) while three animals also received ketoprofen (0.02 ml). Animals were then transported to the MRI suite, fitted with an endotracheal tube and sedated using isoflurane anesthesia. Sedation was maintained using less than 1.5 % isoflurane. Animals were then placed in a stereotaxic device while heart rate, respiration, and oxygen saturation were monitored continuously throughout the procedure. Body temperature and glucose were assessed before and after scanning. All scanning procedures were performed using protocols approved by the University of Wisconsin Institutional Animal Care and Use Committee (IACUC).

For both pre-adolescent and neonatal animals, whole-brain anatomical images were acquired using an axial T1-weighted 3D inversion recovery prepared fast spoiled gradient recalled scan [IR-fSPGR; repetition time (TR) = 11.448 ms, echo time (TE) = 5.412 ms, inversion time (TI) = 600 ms, flip angle $\alpha = 10°$, number of excitations (NEX) = 2, field of view (FOV) = 140 × 140 mm, matrix = 256 × 256 interpolated to 512 × 512, in-plane resolution = 0.27 mm, slice thickness/gap = 0.5/0 mm, 248 slices]. Resting-state functional MRI's were acquired using a T2*-weighted echo planar imaging (EPI) sequence (TR/TE/Flip/FOV/Matrix: 2000 ms/25 ms/90°/140 mm/64 × 64; 26 × 3.1-mm axial slices; gap: 0.5-mm). For the infants, three consecutive repetitions were run of this scan. Diffusion weighted imaging (DWI) was performed using a two-dimensional, echo-planar, spin-echo sequence [TR/TE = 10000/85.3 ms, $\alpha = 90°$, NEX = 1, FOV = 144 × 144 mm, matrix = 128 × 128 interpolated to 256 × 256, in-plane resolution = 0.5625 mm, slice thickness/gap = 1.3/0 mm, 68 interleaved slices, echo-planar spacing = 816 μs. DWI (b = 1000 s/mm^2) was performed in 72 non-collinear directions with 6 non-diffusion weighted images]. Images were acquired in the coronal plane through the entire monkey brain. A co-planar field map was also obtained using a gradient echo with images at two echo times: TE1 = 7 ms, TE2 = 10 ms.

DTI analysis and tractography

Diffusion weighted images were corrected for eddy current distortions using FMRIB Software Library (FSL)'s tools for rigid registration (Woolrich et al. 2009). To account for the movement of individual volumes after this registration the b-vector files were adjusted for the applied registration parameters during the eddy correction. The co-planar field maps were manually skull stripped and then applied to the DWI's using FSL's FUGUE to account for local field inhomogeneities that were encountered in the scanner.

Additional methods were applied to counter increased noise due to the small size of the rhesus primate brain. Voxels with extreme intensities were removed by applying a mask that excluded the upper 1 % of the apparent diffusion coefficient, lower 1 % of the diffusion-weighted map and lower 1 % of the b0 maps. Raw DWI's were smoothed in plane with 0.5 mm smoothing kernel.

The influence of local noise on the tensor calculation was reduced by using a method for robust estimation of tensors by outlier rejection (RESTORE, as implemented in Camino software; Cook et al. 2006). This method uses an average noise estimation to determine which diffusion measurements are extreme outliers and will exclude those values from the computation of the three-dimensional diffusion estimation. This method has been proven to increase reliability of the tensor estimation in particularly noisy datasets (Chang et al. 2005). Fractional anisotropy (FA) measures were calculated to quantify local diffusion measures after fitting the tensors. A population-averaged T1-weighted image was registered to the FA to be used for anatomical reference using FSL's linear registration tool (FLIRT).

Deterministic fiber tractography was run to model white matter fiber pathways from the measured local diffusion directions. Whole-brain fiber tractography was performed using Camino software (Cook et al. 2006) that implemented a tensor deflection (TEND) algorithm for optimal estimation of the fiber tracking directions (Basser et al. 2000; Lazar et al. 2003). Fiber tracking was terminated in voxels where FA was below 0.15. Visualization software (Wang et al. 2007) was used to iteratively delineate the fiber pathway of interest using anatomically defined waypoints. This study aimed to delineate the tracts connecting the dorsal amygdala to the BSTL by placing a waypoint in the region of the posterior dorsal amygdala (containing the

Ce, at the rostrocaudal level where the amygdala-hippocampal junction is best seen Fig. 1), and a second waypoint in the region surrounding the anterior commissure just lateral to the midline that contained the BSTL (see Fig. 1). Since the fornix travels in parallel and in close proximity to the ST, "NOT" points were also used to exclude fornical fibers originating in the hippocampus; additional "NOT" points were used to exclude crossing fibers and fibers of the longitudinal fasciculus. Intra-individual images at 3-weeks and 7-weeks were spatially registered together using tensor based normalization methods (DTI-TK; Zhang et al. 2006). The ST/VA tracts were converted to a binary mask, mean FA for the entire tract was extracted, and paired-sample *t* tests were used to examine differences across developmental time points.

Resting state data analysis

Dorsal amygdala (Ce region) functional connectivity in the infant monkeys was assessed with methods previously used in adolescent humans (Oler et al. 2012), and a large sample of preadolescent monkeys (Birn et al. 2014; Oler et al. 2012). fMRI scans were performed using methods modified from prior work demonstrating the reliability of collecting resting fMRI data in anesthetized rhesus monkeys (Vincent et al. 2007). All processing steps were carried out in AFNI (Cox 1996), unless otherwise indicated. Anatomical scans were manually skull stripped with SPAMALIZE (http://psyphz.psych.wisc.edu/~oakes/spam/spam_frames.htm). The skull stripped anatomical scans were registered to a rhesus macaque template made from 592 pre-adolescent monkeys (0.625 mm isotropic voxels) utilizing AFNI's nonlinear registration program 3dQwarp with a minimum patch size for warp searching set at the minimum of 9 mm, and the "workhard" option, which allows for more iterations, and is helpful in cases when the volumes are hard to align, as is the case in these infant scans. Resting state scans (collected in three 5-min runs) were slice timing and motion corrected, had the first 4 frames removed, and were adjusted for field inhomogeneities with a field map correction. The preprocessed resting state scans were warped into the standard space with the warps calculated from the anatomical scans, and up-sampled to anatomical resolution. In order to reduce the influence of non-neuronal fluctuations on functional connectivity estimates, average signal intensity time courses from the white matter (WM) and cerebral spinal fluid (CSF) were regressed out of the EPI time series (Jo et al. 2010). The residualized resting state signal was further processed with a 4 mm Gaussian blur and temporal bandpass filtering (low = 0.01 Hz, high = 0.1 Hz). Analysis of the group level connectivity was performed with AFNI's 3dGroupInCorr, by placing a 2 mm seed ROI in the right dorsal amygdala region. A temporal correlation analysis was run with the seed mean time-series using all available data, while controlling for age and subject. The resulting connectivity data was corrected for multiple comparisons testing with false detection rate (FDR) methods ($q = 0.05$). As in the previously published study (Oler et al. 2012), the current analysis was restricted to examine the connectivity of a right dorsal amygdala seed. To examine developmental changes in extended amygdala functional connectivity, the Fisher's *Z* transformed connectivity values were extracted from the right BSTL cluster resulting from the FDR corrected main-effects connectivity map. A linear mixed effects model was used to examine the influence of age (3 vs. 7 weeks) on the extracted mean connectivity values from all available pairs of scan data, while taking the within-subjects and by scan variance into account. In addition we ran a non-parametric Wilcoxon rank sum test to examine changes in Ce-BST connectivity between 3 and 7 weeks. This test does not assume normally distributed data, which is an assumption that might get violated in tests with a small sample size.

Tract tracing studies and methods

Subjects

Eight adolescent male primates (*Macaca fascicularis* and *Macaca nemestrina*) (2–3 years old) weighing between 2.5 and 4.9 kg were used at the University of Rochester (World Wide Primates, Tallahassee, FL, USA; Three Springs Laboratories, Pekaski, PA, USA; Labs of Virginia, Yemassee, SC, USA; Alpha Genesis, Yemassee, SC, USA). All experiments were carried out in accordance with National Institute of Health guidelines. Experimental design and techniques were aimed at minimizing animal use and suffering and were reviewed by the University of Rochester Committee on Animal Research.

Defining the central extended amygdala regions in primates

In human and nonhuman primates, the BSTL and Ce have several subdivisions that have been described using various terminologies (de Olmos 2004; Freedman and Shi 2001; Gaspar et al. 1987; Heimer et al. 1999; Kaufmann et al. 1997; Lesur et al. 1989; Martin et al. 1991; Walter et al. 1991). Our immunostaining results are consistent with previous work and we use the terminology of de Olmos (1990) and Heimer et al. (1999) for all subregions. Sets of subdivisions in the primate BSTL 'mirror' others in the Ce. The BSTL and Ce each have transition zones with the striatum, which like the striatum, are demarcated by relatively higher levels of acetylcholinesterase (AChE) staining; these include the juxtacapsular subdivision of the BSTL (BSTLj), 'mirrored' by the lateral amygdalostriatal transition zone (Astr) flanking the Ce, and the thin capsular regions of the BSTL

and Ce (BSTLc and CeLc, respectively). In contrast, the BSTLcn and CeLcn are most easily visualized based on relatively low AChE staining in each, and very strong staining for several neuropeptides, including somatostatin and enkephalin (see deCampo and Fudge 2013 for details). Surrounding the BSTLcn and CeLcn in some sections, are smaller islands, separated by fibers of the passing ST. These are presumed to be parts of the BSTLcn and CeLcn that are divided away from the main subnucleus by the passing fiber bundles. Finally, the BSTLP and the CeM are both composed of heterogeneous cell types, demonstrate moderate AChE staining, and are largely continuous with the SLEAc (Martin et al. 1991). Importantly, the BSTLP, CeM and SLEAc—along with cholinergic cell islands—are all pierced by the VA fiber tract as it courses along the basal forebrain.

Injection sites

To determine BSTL-SLEAc-Ce connectivity in the same animal, we (JF, BB and DdC) employed a strategy using bidirectional tracer injections into the BSTL and Ce 'poles' of the EAc (Fig. 2). Small injections (40 nL) of the bidirectional tracers, Lucifer yellow conjugated to dextran amine (LY; 10 %, Molecular Probes, Eugene, OR, USA), tetramethylrhodamine, conjugated to dextran amine ('fluoruby', FR; 4 %, Molecular Probes), and fluorescein conjugated to dextran amine (FS; 10 %, Molecular Probes) were stereotactically injected into the BSTL and Ce. Additionally, several injections of the tracer wheat-germ agglutinin-horse radish peroxidase (WGA; 10 %, Sigma, St. Louis, MO, USA), which has retrograde but not anterograde properties in primate, were also made for comparison. Control injections of all tracers were placed in the nearby striatum. Previous studies from the Fudge laboratory have indicated that there is no cross-reactivity of antibodies to FR, FS, WGA and LY. In our hands, FR, FS, and LY have similar anterograde and retrograde properties, and are sensitive indicators of terminal fields when survival is between 10 and 14 days (Cho et al. 2013; Haber et al. 2000). WGA results in relatively more labeled cells compared to a similar-sized injection of FR, FS, and LY, however, the distribution of labeled cells is the same. The location and extent of Ce and BSTL tracer injections examined in this study are presented in Fig. 2 and Table 1.

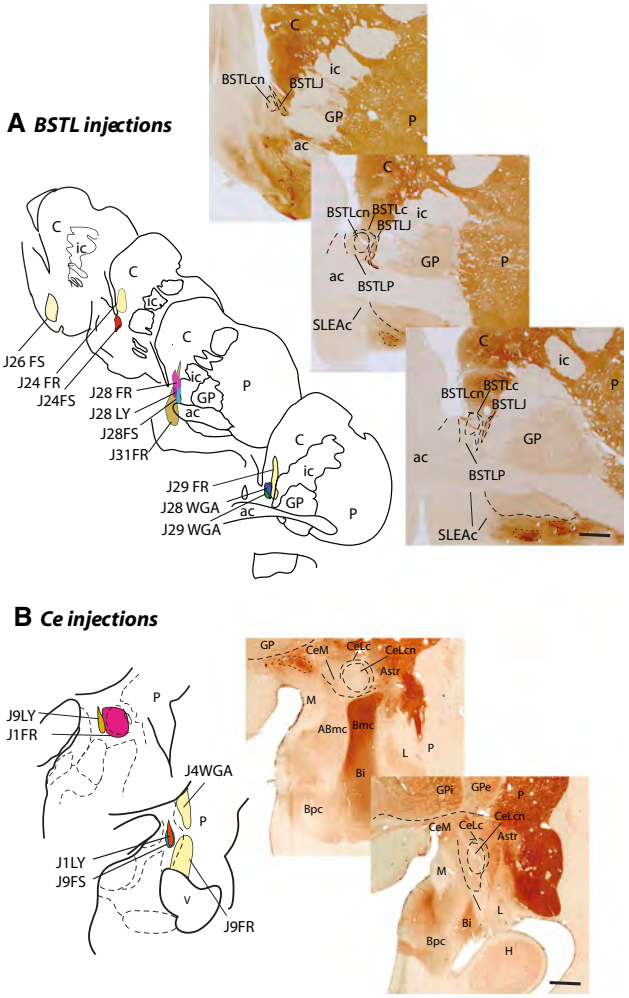

Fig. 2 *Top* **a** BSTL injection sites. Schematized drawings of various injection sites in the BSTL with control injections in or encroaching on the striatum in *light yellow*. To the right are acetylcholinesterase (AChE) stained sections at similar levels showing BSTL subregions. *Bottom* **b** Ce injection sites. Schematized drawings of various injection sites in the Ce with control injections in the amygdalostriatal transition zone and striatum in light yellow. AChE stained sections to the right show the Ce subregions. *Scale bar* 1 mm

Technical considerations for tracing studies

Several limitations of these tract-tracing studies should be mentioned. Together, retrograde and anterograde studies are powerful tools to analyze neural pathways at a cellular level. Retrograde studies provide a sensitive overview of afferent sub-structures that can influence specific brain regions. Anterograde studies are critical for interpretation of the retrograde data, since the density of retrogradely labeled cells does not necessarily correspond to the density of the terminal field. However, issues such as encroachment of tracer on nearby structures, and the possibility of tracer uptake and transport by 'fibers of passage' and axon collaterals, leading to false-positive results, are concerns for all types of tracers (Halperin and LaVail 1975; Nance and Burns 1990). These issues are particularly relevant for injections in structures such as the BSTL and Ce, which are small and lie in, or near, passing fiber tracts. To minimize these problems, we used very slow injections of tracer (Nance and Burns 1990; Schmued et al. 1990; Vercelli et al. 2000), and eliminated cases where there was non-

Table 1 Relative placement of tracer injections into BSTL and Ce subdivisions and adjacent striatum

	BSTLcn	BSTLP	BSTLJ/BSTLc	Striatum
J24FS	+++	+	+	
J28WGA	+++	+	++	
J29WGA	+++	+	+	
J31FR	+	+++	+	+++
J28LY	+	+	+	
J28FS			+++	
J28FR			+++	++
J29FR			+++	+++
J26FS				+++
J24FR				+++
	CeLcn	CeM	CeLc/Astr	Striatum
J1LY	+++			
J1FR	+++	++		
J9FS	+++	+		
J9LY		+++		
J9FR			+++	+
J4WGA				+++

specific labeling. We analyzed remaining cases by their inputs and outputs to other structures. For example, fibers leaving the amygdala and 'passing through' the BSTL and Ce go on to innervate the cortex and mediodorsal thalamus (Aggleton and Mishkin 1984; Miyashita et al. 2007; Porrino et al. 1981; Russchen et al. 1987). While we noted retrogradely labeled cells in the cortex, their distribution was confined to areas previously noted to innervate the BSTL (Freedman et al. 2000; Ghashghaei and Barbas 2001) and Ce (Stefanacci and Amaral 2002), rather than the broader cortical regions that innervate the basal and accessory basal nuclei (Cho et al. 2013). Additionally, there were few to no labeled cells or fibers in the mediodorsal thalamus, indicating that uptake by fibers en route to the basal and accessory basal nuclei was minimal (Aggleton and Mishkin 1984; Porrino et al. 1981; Russchen et al. 1987). Similarly we found that injection sites that included the BSTLcn, BSTLP, CeM, and CeLcn resulted in retrogradely labeled cells in the parabrachial nucleus (Pritchard et al. 2000), whereas injections outside of these areas in the BSTLJ or the striatum did not. Injection sites spreading into the striatum invariably resulted in labeled fibers in the globus pallidus or retrogradely labeled cells in mediodorsal thalamus (Russchen et al. 1987).

Surgery

To minimize animal use, many injections were performed as parts of other studies (deCampo and Fudge 2013; Fudge et al. 2004, 2012; Fudge and Tucker 2009). Stereotaxic coordinates were determined prior to injection using MRI imaging (3 T, coronal sections, 0.8 mm thick, 0.1 mm apart), using previously described techniques (deCampo and Fudge 2013).

Two weeks after surgery, animals were deeply anesthetized and euthanized by perfusion through the heart with 0.9 % saline containing 0.5 ml of heparin sulfate (200 ml/min for 10 min), followed by cold 4 % paraformaldehyde in a 0.1 M phosphate buffer/30 % sucrose solution (100 ml/min for 1 h). The brain was extracted from the skull, placed in a fixative overnight, and then put through increasing gradients of sucrose (10, 20, and 30 %). Brains were cut on a freezing microtome (40 μm) and all sections were stored in cryoprotectant solution (30 % ethylene glycol and 30 % sucrose in 0.1 M phosphate buffer) at −20 °C (Rosene et al. 1986).

Immunocytochemistry

1:8 sections through the brain were immunostained for tracer. Sections were rinsed in 0.1 M phosphate buffer (pH 7.2) with 0.3 Triton-X (PB-TX) and treated with peroxidase inhibitor for 5 min, followed by more rinses in 0.1 M PB-TX. Sections were then preincubated in a blocking solution of 10 % normal goat serum (NGS) in 0.1 M PB-TX for 30 min. Tissue was placed in primary antisera to LY (1:2000, Molecular Probes, rabbit), FS (1:2000, Molecular Probes, rabbit), FR (1:1000, Molecular Probes, rabbit), and WGA (1:2000, Sigma, rabbit) for 96 h at 4 °C. After thorough rinsing with 0.1 M PB-TX, and preincubation with 10 % NGS-PB-TX, sections were incubated in biotinylated secondary anti-rabbit antibody. Tracers were visualized using avidin–biotin reaction (Vector ABC Standard kit, Burlingame, CA, USA). Additional compartments for each case were processed for tracer, nickel intensified, and counterstained with AChE, cresyl violet, or calcium binding protein immunoreactivity (CaBP-IR). Detection of these tracer molecules in tract tracing has been extensively documented (see "Technical considerations for tracing studies", "Discussion").

Histological analysis

Injection sites

The relative position of each injection site within subdivisions of the BSTL or Ce was confirmed by charting 1:8 sections through the basal forebrain, with reference to adjacent sections immunostained for various peptide markers, and AChE. Injection sites that encroached on the globus pallidus, internal capsule or other fiber tracts were eliminated from the analysis. We also analyzed the

accuracy of injection site placement by inspecting the pattern of projections to or from other brain regions based on the literature. Injection sites were classified as being in the BSTL or Ce if they resulted in labeled cells and fibers in the parabrachial nucleus and the midline thalamic nuclei (Price and Amaral 1981; Pritchard et al. 2000), but did not result in labeled fibers in the globus pallidus (Haber et al. 1990), subthalamic nucleus (Carpenter et al. 1981), and mediodorsal thalamus (Price and Amaral 1981). Injection sites that encroached on the striatum or globus pallidus invariably had labeled fibers terminating, respectively, in the CaBP-IR globus pallidus or subthalamic nucleus. Several example photomicrographs of the tracer injection sites from individual BSTL or Ce injections are presented in Fig. 3.

Charting the distribution of labeled cells and fibers

The distribution of retrogradely labeled cells was determined under brightfield microscopy with a 10× objective, assisted by Neurolucida software and a mechanized stage (Microbrightfield Bioscience, Williston, VT, USA). All charts were imported into Canvas 14 and saved. The charts of adjacent neuropeptide-labeled sections were also drawn and converted into Canvas 14, where they were superimposed onto tracer-labeled sections in transparent layers, and carefully aligned using landmarks. The bidirectional properties of FR, LY, and FS allowed us to also chart the distribution of anterogradely labeled fibers resulting from these injections. For anterograde labeling, charts were drawn on paper using camera lucida techniques under darkfield illumination (10×), with care taken to chart only fine, thin processes containing synaptic boutons. Paper charts were then scanned as high resolution as TIFF files, and converted to line drawings in Canvas 14. Digitized charts of anterogradely labeled fibers for each case were superimposed in yet another transparent layer over adjacent maps of histologically stained sections, and carefully aligned using landmarks. This allowed creation of individual maps through the extended amygdala for each injection site. Several example photomicrographs of labeled cells and fibers from individual subjects are presented in Fig. 3.

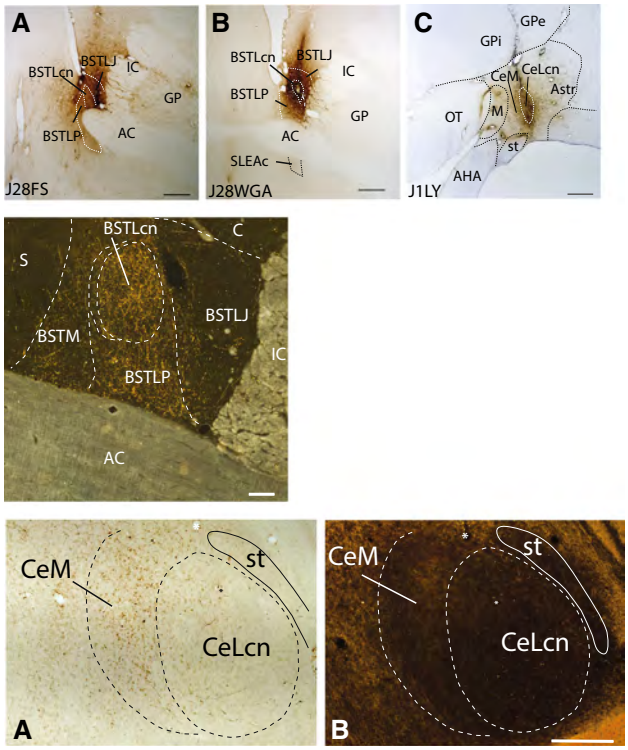

Fig. 3 *Row 1* **a**, **b** photomicrographs of representative injections into the BSTL (J28FS and J28WGA). Nuclear subdivisions were determined from adjacent sections stained for AChE. Case J28FS is centered on the BSTLJ and Case J28WGA is centered on the BSTLcn. **c** A photomicrograph of an injection into the CeLcn (Case J1LY) with light cresyl *violet* counterstain. Note that the gliotic scar dorsal to injections site is due to DAB stain; there is no tracer uptake there. *Scale bar* 1 mm. *Row 2* photomicrograph under dark-field illumination showing the distribution of labeled fibers in the BSTL subdivisions resulting from Case J9LY. *Scale bar* 500 μm. *Row 3* **a** A brightfield image of retrogradely labeled cells in the CeN subdivisions following an injection in the BSTL (Case J24FS). **b** A darkfield image of an adjacent section stained with AChE to determine Ce subdivisions. The *asterisks* show nearby blood vessel landmarks. *Scale bar* 500 μm

Results

Tract-tracing studies

Neuronal tract tracing studies allowed us to first map point-point connections, and the directionality of projections, between the anatomical subdivisions of Ce and BSTL. In addition, we were able to visualize the scope and complexity of local circuitry within the entire EAc trajectory. We charted the organization of labeled neural elements, i.e. labeled cells and presumptive terminating fibers (thin, beaded fibers), rather than passing white matter tracts. These studies formed a basis for interpretation of the developmental in vivo studies in infants using DTI and resting state fMRI.

Ce efferent pathways

We first examined the Ce → BSTL pathway based on retrogradely labeled cells found in the Ce and SLEAc. Eight injections were placed in the BSTL region (Fig. 2a; Table 1). Analysis revealed that these injections covered various BSTL sub-nuclei (e.g., BSTLcn, BSTLP, BSTLJ/BSTLc). Three of these injections (J31FR, J29FR, J28FR)

straddled the striatum and BSTL. Comparison injections in the ventral striatum (case J26FS) and ventral caudate nucleus (case J24FR) were also examined (results not shown).

Injections that included the BSTL resulted in retrogradely labeled cells in Ce and SLEAc. All BSTL injections resulted in labeled cells in the CeM, which formed a continuous stream into the SLEAc (Fig. 4a–c). Injections involving the BSTLcn subdivision (J24FS, red, J29WGA green, and J28WGA, blue) resulted in additional labeled cells in the CeLcn. Retrogradely labeled cells in the SLEAc were mainly CaBP-negative medium-sized neurons (i.e. non-cholinergic neurons). A control injection into the shell of the ventral striatum also resulted in labeled cells (not shown in Fig. 4) in the CeM and SLEAc consistent with previous results, and suggesting a 'transitional' role for the shell of the nucleus accumbens between striatopallidal and EAc systems (deCampo and Fudge 2013; Fudge et al. 2002).

Anterogradely labeled fibers in the BSTL and SLEAc resulting from injections in the Ce confirmed the retrograde results. Five injections were placed in the region of the Ce (Fig. 2b; Table 1). Of these, one injection (J9FR) straddled the striatum and CeLc/Astr. All injection sites involving the Ce resulted in patches of anterogradely labeled fibers in the SLEAc, BSTL and shell of the ventral stratum (Fig. 4d–f). Labeled fibers in the SLEAc consisted mostly of very fine, beaded fibers that avoided the globus pallidus (Fig. 4g), although thick non-varicose passing fibers (i.e. non-terminating fibers comprising the VA bundle, not charted) were also present. Most finely beaded fibers avoided the cholinergic cell bodies, which are also embedded in the fibers of the VA bundle, and terminated densely in the surrounding neuropil, suggesting contacts on the broad dendritic arbors of the cholinergic system. Injections that included the CeM (J9LY and J1FR) resulted in the most labeled fibers in the SLEAc and in all BSTL subdivisions, whereas injections confined to the CeLcn had a lighter concentration of labeled fibers. Cases J1LY and J9FS, which were confined to the CeLcn had the lightest distribution of the labeled fibers that overlapped the BSTLcn, and spread into the BSTLP and contiguous SLEAc. Control injections into the caudal ventral striatum (case J9FR) did not reach the SLEAc, and instead overlapped the caudal ventral globus pallidus (not shown), indicating that they are excluded from EAc intrinsic circuits.

BSTL efferent pathways

We next examined the opposite pathway, first charting the distribution of retrogradely labeled cells in the BSTL and SLEAc that resulted from the Ce injections described above. Surprisingly, there were almost no labeled cells in the BSTL following all Ce injections (Fig. 5a–c); the few that were found were in the BSTLP. In contrast, there were many labeled cells in the SLEAc after all injections, which flowed in a continuum from the CeM. The highest numbers of labeled cells in the SLEAc resulted from the injections that included the CeM, supporting the concept of the continuity of these areas found in cytoarchitectural and histochemical work.

In the anterograde direction, all BSTL injections involving bi-directional tracer resulted in dense, discontinuous patches of labeled thin, highly beaded fibers in the SLEAc (Fig. 5d–f). The densest patches of labeled fibers frequently surrounded, rather than directly overlapped, the cholinergic cell islands (not shown). However, individual labeled fibers could be seen in close apposition to proximal dendrites of the large cholinergic neurons. The density of anterogradely labeled fibers tapered off sharply at caudal levels, leaving a relatively light concentration of labeled fibers in the Ce, based on both composite analyses and when examining individual cases (see Fig. 5g). For example, the injection in case J31FR resulted in relatively more labeled fibers in the Ce compared to other BSTL injections, but the overall density of labeled fibers was still relatively sparse, and largely restricted to the CeM (Fig. 5g). The injection into the shell of the ventral striatum (case J26FS) also resulted in labeled fibers in the SLEAc, which extended into the CaBP-positive globus pallidus, but did not extend into the Ce (not shown). As expected, a control injection into caudate nucleus (case J24FR) only resulted in labeled fibers in the globus pallidus (not shown).

Development of white matter tracts using DTI in infant monkeys

Deterministic tractography in preadolescent monkeys demonstrates the ability of DTI to detect the white matter pathways connecting the dorsal amygdala Ce-region to the BSTL region (Fig. 1). Employing similar methods used to delineate the VA and ST pathways in the sample of preadolescent monkeys, Fig. 6 presents the deterministic tractography of the VA and ST at 3 and 7 weeks of age. The results confirm that these pathways are present very early in life, as the VA and the ST are observed coursing through and linking extended amygdala subregions in each infant subject at both time points. Paired-samples *t* tests did not detect any significant differences between 3 and 7 weeks of age in mean FA, or mean diffusivity measures, extracted from the tracts (p's > 0.60).

Development of Ce-BST functional connectivity (fMRI) in infant monkeys

Our previously published data in a large sample of older preadolescent monkeys (Oler et al. 2012) demonstrated highly significant functional connectivity between right Ce

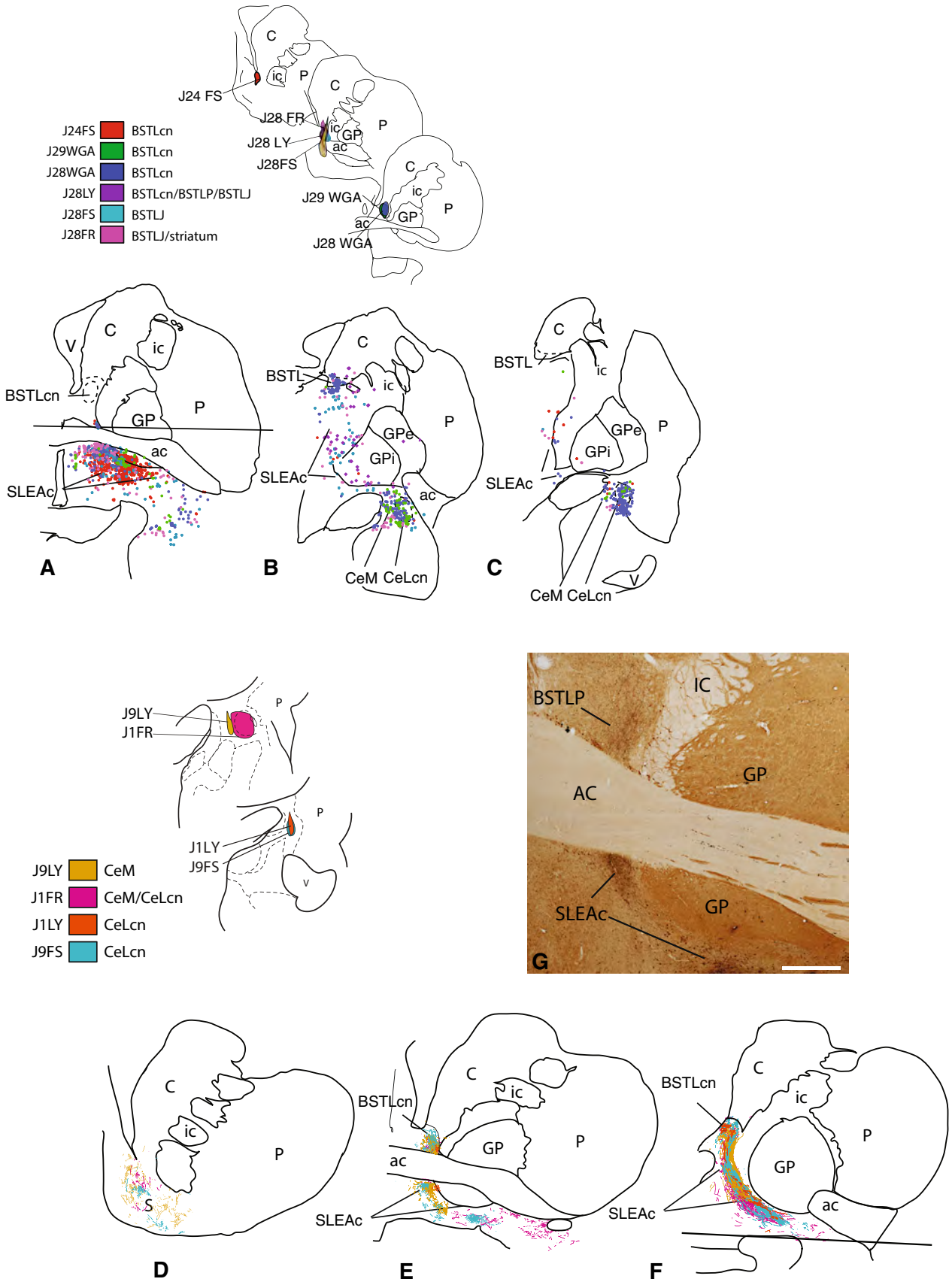
J24FS BSTLcn
J29WGA BSTLcn
J28WGA BSTLcn
J28LY BSTLcn/BSTLP/BSTLJ
J28FS BSTLJ
J28FR BSTLJ/striatum
J24 FS
J28 FR
J28 LY
J28FS
J29 WGA
J28 WGA
C
ic
P
GP
ac
V
BSTLcn
SLEAc
BSTL
GPe
GPi
CeM CeLcn
A
B
C
J9LY
J1FR
J1LY
J9FS
J9LY CeM
J1FR CeM/CeLcn
J1LY CeLcn
J9FS CeLcn
BSTLP
IC
AC
G
D
E
F

◀**Fig. 4** Ce → BSTL projection viewed from composite retrograde (*top*) and anterograde perspectives (*bottom*). Injections into the BSTL result in many labeled cells in the SLEAc and Ce (*top* **a**–**c**). Ce injections (*bottom*) result in many thin varicose fibers throughout the BSTL (*bottom* **e**, **f**) as well as in the shell of the ventral striatum (**d**) and SLEAc (**e**, **f**). The areas above and below the *horizontal lines* in (**a**) and (**f**) contained injection sites and were not charted. **g** Photomicrograph of dense concentrations of labeled fibers (*black*) in the BSTLP and SLEAc following injection in case J9LY. The *light brown* staining is CaBP-ir, which is high in the globus pallidus and the cholinergic cells. *Scale bar* 1 mm

and bilateral BST regions, as well as a homologous region of the contralateral (left) amygdala. To examine Ce-BST functional connectivity in the infant monkeys, we used a right dorsal amygdala seed to extract the mean time-series and ran a voxelwise temporal correlation analysis. Combining all the usable infant fMRI data across 3 and 7 weeks of age we found significant ($q = 0.05$, FDR corrected) positive functional connectivity with the right BST region and the contralateral amygdala (see yellow clusters in Fig. 7a and Table 2). At a threshold of $p = 0.005$, uncorrected, we also found connectivity between right dorsal amygdala and left hemisphere SLEAc and bilateral BST regions (see dark orange clusters in Fig. 7a).

Interestingly, a comparison between 3 and 7 weeks of age revealed age-related changes in Ce-BST functional connectivity with significantly greater connectivity at 7 as compared to 3-weeks ($p < 0.032$). Results of the Wilcoxon rank sum test were consistent with the earlier analysis ($W = 3$, one-tailed, p value $= 0.028$). Collectively, these results suggest that DTI-detectable fiber tract connections between Ce and BST exist at birth and that changes in Ce-BST functional integration occur over the first 2 months of life (Fig. 7b).

Discussion

Here, we used complementary ex vivo and in vivo tools to characterize patterns of intra-extended amygdala connectivity and its early-life development. These ex vivo data inform our imaging studies that examine structural and functional connectivity by providing insight into the directionality of intra-extended amygdala connections. Moreover, our longitudinal imaging in very young monkeys indicates that although the main fiber tracts linking the Ce and BST are in place shortly after birth, these pathways are undergoing functional development during the first months of life. Together these ex vivo tracing studies and in vivo imaging studies provide important complementary insights into the nature of EAc connectivity and how it comes to be.

There were two main findings resulting from the tracer injection studies that allowed us to gain further insight into the directionality and anatomical resolution of the imaging data. Both the retrograde and the anterograde data indicate that the direct projection from the Ce to the BSTL is relatively heavier than the reverse path. This relative directionality has not been previously documented in the primate, and most rodent data use small anterograde injections to reveal one arm of the pathway in separate animals (Dong et al. 2001a, b; Dong and Swanson 2004a, b; Sun et al. 1991). A bi-directional study in the rodent, reported in a review (Zahm 2008), used deposits of biotinylated dextran amine into the Ce and BST in separate cases to compare the anterograde labeling in the two structures. Results seemed to indicate a Ce >BST directionality (as well as robust associational inputs throughout the SLEAc), similar to both the retrograde and anterograde findings reported here in the monkey (cf. Fig. 2 in Zahm 2008). In our work, we also find that the SLEAc stands out in receiving and sending abundant projections to both the BSTL and Ce. The robust interconnections between the SLEAc and both poles of the EAc underscore the SLEAc's importance as a communication hub, and that Ce and BSTL function cannot be considered without it (Fig. 8). This is a factor that should be taken into account in human functional studies.

The tract tracing results suggest that the direct Ce to BSTL inputs are likely more influential than the reverse path in driving the activity responsible for the strong functional connectivity between these extended amygdala structures that is observed in our in vivo studies. However, this connectivity could theoretically be a result of direct inputs from a third structure projecting to both BST and Ce, such as the SLEAc, amygdala proper, or the anterior hippocampus. With regard to the functional connectivity between dorsal amygdala Ce-region and SLEAc, our previous study with a sample of 107 preadolescent monkeys (Oler et al. 2012) found significant functional connectivity between the Ce and the substantia innominata region containing the SLEAc. This finding was also observed in the present study of infant monkeys (see Fig. 7a). Interestingly, in our previous study we found that Ce-BST connectivity was significantly greater than Ce-SLEAc connectivity (Oler et al. 2012). The relatively lower Ce-SLEAc functional connectivity (as compared to Ce-BST connectivity) could be related to the heterogeneity of the cell types within the substantia innominata, the nature of the underlying projection could be different, or there could be different network properties such as recurrent vs. direct projections.

Intrinsic connections of the EAc

A cornerstone of the 'extended amygdala' concept, which is based largely on studies in rats, is that reciprocal,

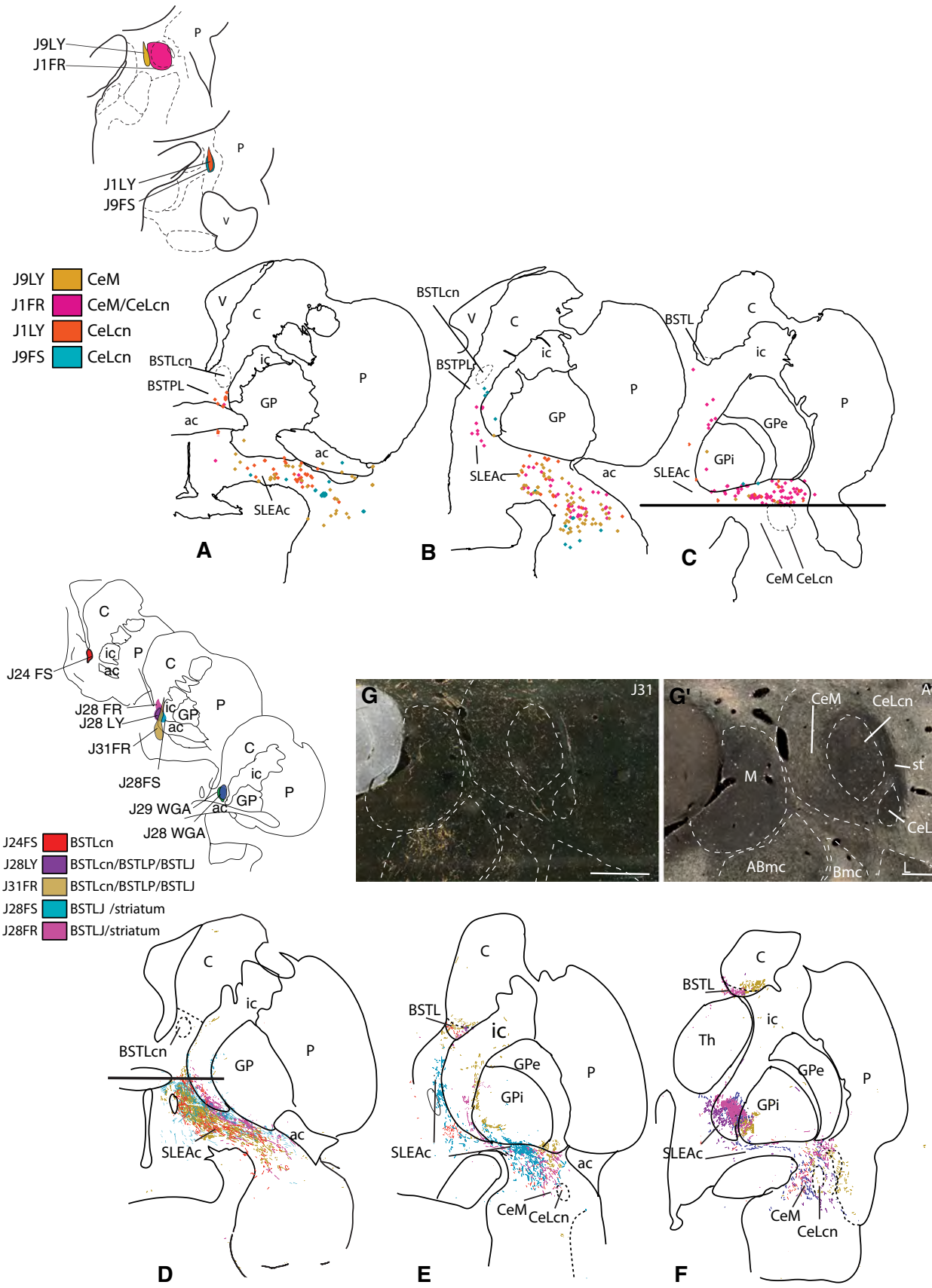
J9LY
J1FR
J1LY
J9FS
P
V
J9LY CeM
J1FR CeM/CeLcn
J1LY CeLcn
J9FS CeLcn
BSTLcn
BSTPL
ac
ic
C
GP
SLEAc
A
B
C
BSTL
GPe
GPi
CeM CeLcn
J24 FS
J28 FR
J28 LY
J31FR
J28FS
J29 WGA
J28 WGA
J24FS BSTLcn
J28LY BSTLcn/BSTLP/BSTLJ
J31FR BSTLcn/BSTLP/BSTLJ
J28FS BSTLJ /striatum
J28FR BSTLJ/striatum
G
J31
G'
AChE
CeM
CeLcn
st
M
CeLcnpc
ABmc
Bmc
L
D
E
F
Th

◀**Fig. 5** BSTL → Ce projection viewed from composite retrograde (*top*) and anterograde perspectives (*bottom*). Retrograde injections into the Ce subdivisions result in relatively few labeled cells in the BSTL but moderate to dense labeled cells in the SLEAc (*top*, **a**–**c**). Anterograde injections into the BSTL result in many labeled fibers in the SLEAc corridor (**d**–**f**) which taper off to form a relatively lighter distribution in the Ce (**f**). Areas below and above *horizontal lines* in (**c**) and (**d**) were not charted due to presence of injection site. **g** Photomicrograph in one case (J31FR) emonstrating the relatively light concentration of labeled fibers in the Ce. **g**′ AChE stained section adjacent to section in **g**, showing the boundaries between amygdala nuclei. *Scale bar* 1 mm

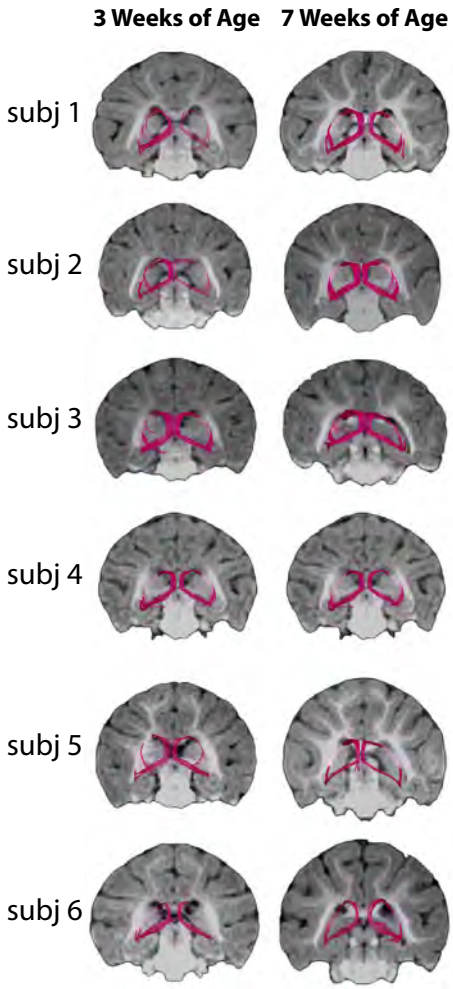

Fig. 6 Visualization of the stria terminalis (ST) and ventral amygalofugal (VA) pathways in neonates using deterministic tractography. The same method used to delineate the ST and VA pathways in preadolescent animals was applied to the scans from infant monkeys. Note that the ST, which in these 3D renderings travels caudally behind the MRI slice and then arches dorsally and rostrally back out in front of the MRI, and the VA pathways were detected in each of the subjects at the 3-week and 7-week time points

associational pathways link the BSTL and Ce structures (Cassell et al. 1999; de Olmos and Ingram 1972; Grove 1988a). The extended amygdala concept has nonetheless remained controversial, with some investigators considering these structures differentiated components of a striatopallidal projection system, rather than a unique macrostructural system (Swanson 2003). Swanson and colleagues felt that the differences between the striatopallidal system and the rest of the basal forebrain (i.e. the structures here cited as EAc) were minor and that it was more useful to conceptualize the whole basal forebrain as consisting of striatopallidal elements, with the Ce and BST as 'differentiated' striatopallidum. The fundamental striatopallidal structure of the 'extended amygdala' was acknowledged in the original descriptions of the extended amygdala (Alheid and Heimer 1988, see page 26), which also cited similar observations by Fallon and Loughlin (1987) and Turner and Zimmer (1984). However, the density of the associational, intrinsic network linking the entire structure was thought to be one unique feature setting the EAc apart from the striatum and pallidum. Although we found uneven reciprocity in direct long paths linking the BSTL and Ce, the prominent position of the SLEAc as a major conduit and integrator of both Ce and BST information, is consistent with the concept of the EAc (Alheid and Heimer 1988; Grove 1988a; McDonald 2003). In primates, there does not seem to be a cellular or histochemical boundary between the CeM, SLEAc and BSTLP (de Olmos 2004; Martin et al. 1991), and our results support this idea on connectional grounds. All injections in either the Ce or BSTL resulted in both labeled cells and fibers that flowed in a continuous stream along the CeM/SLEAc/BSTLP subregions. The continuity of the CeM, SLEAc and BSTLP is also supported by previous work documenting that these regions have parallel outputs to effector targets such as the periaqueductal gray, the substantia nigra, lateral parabrachial nucleus and solitary nucleus in the rat (Bunney and Aghajanian 1976; Gray and Magnuson 1987, 1992; Grove 1988a; Moga et al. 1990; Rizvi et al. 1991) and the monkey (Fudge and Haber 2000, 2001).

Limitations and technical considerations

Projections from other regions, including other amygdalar nuclei that target the BST (e.g., from the basolateral complex), also travel along the ST and VA en route to the BST. The present DTI tractography methods cannot distinguish between these fibers and those targeting the BST that originate from Ce neurons. Furthermore, it should be noted that caution must be used when comparing tract-tracing and tractography data. Because of the properties of water diffusion the latter is better at showing myelinated fibers, of which probably more in the ST and VA arise from the basolateral complex than the EAc. Thus, these two components of the present study could be emphasizing

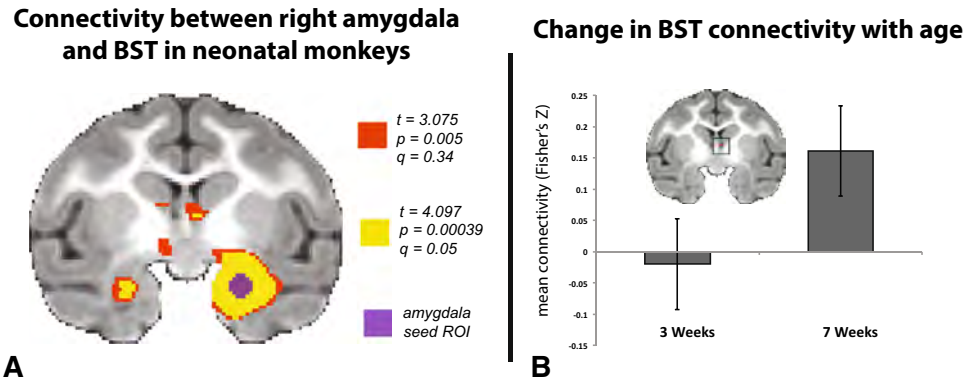

Fig. 7 Ce-BST functional connectivity (fMRI) in infant monkeys. **a** Group temporal correlation map of dorsal amygdala Ce-region functional connectivity in infant rhesus monkeys. fMRI time-series data were collected while the animals were under anesthesia, and the right dorsal amygdala region (*purple*) was seeded for group connectivity analysis. The resulting connectivity data was corrected for multiple comparisons testing with false detection rate (FDR) methods ($q = 0.05$, *yellow*). **b** Developmental changes in Ce-BST connectivity were assessed by extracting the mean connectivity values from the FDR-corrected BST cluster in the right hemisphere, and running a linear mixed effects model to examine the influence of age on the mean connectivity, while taking the within-subjects and by scan variance into account. Right BST connectivity with right dorsal amygdala significantly increases between 3 and 7 weeks of age ($p < 0.032$)

Table 2 Significant functional connectivity of the infant dorsal amygdala

Anatomical location of cluster	Hemisphere	No. of voxels	*x*	*y*	*z*	Peak *t* value
Amygdala	Left	190	−11.875	0.625	−10.000	5.61
Superior temporal gyrus	Left	45	−20.000	1.875	−11.250	5.50
SLEAc/lateral hypothalamus	Left	20	−3.125	−1.250	−1.250	4.60
Superior colliculus	Right	10	1.875	−17.500	0.625	−4.45
Temporal area TE, occiptomedial part	Right	8	25.000	−20.000	5.625	4.50
BSTL region	Right	6	1.875	0.000	2.500	4.41
Anterior cingulate cortex (BA32/24)	Right	6	1.875	20.625	10.000	4.21
Occipital cortex (area V4)	left	2	−28.125	−25.625	−8.750	4.20

A 2 mm seed region was placed in the region of the right dorsal amygdala, and the mean time series was extracted and regressed against the rest of the brain. Overall mean connectivity was assessed while controlling for age and subject. The temporal connectivity was Fisher'-z transformed and thresholded using FDR methods ($q = 0.05$, $p = 0.00039$) resulting in 8 clusters listed above in descending order by size. The anatomical location of the cluster, the hemisphere, and the coordinates relative to the anterior commissure are presented, along with the peak *t* value for each cluster

different fiber systems. Finally, recent multisynaptic viral tracing studies in the rodent demonstrated a very complex network of intra-BST circuits connecting medial and lateral parts of the BST (Bienkowski et al. 2013). To gain a clearer picture of the intrinsic connectivity of these structures in the non-human primate, future studies should investigate the second-order 'cross-talk' between the different components of the EAc and the hypothesized 'medial division of the extended amygdala' (medial amygdala nucleus and medial nuclei of the BST).

Development of extended amygdala circuits

In vivo imaging in monkeys revealed that the poles of the primate EAc (i.e. the Ce and BSTL) are structurally connected via the ST and the VA by 3 weeks of age (Fig. 6, left column). This finding is not surprising considering evidence that the ST is a detectable tract in the fetal brain (Huang et al. 2009; Rose et al. 2014; Vasung et al. 2010). Analysis of the change in ST/VA FA from 3 to 7 weeks did not detect significant differences, however, considering the relatively small sample in the present study caution should be used not to over-interpret these null findings. Future studies will be needed to generate much larger developmental data sets in the nonhuman primate to either refute or confirm the DTI observations reported here.

Resting state functional connectivity when performed in anesthetized animals is referred to as 'intrinsic connectivity' (Vincent et al. 2007). Variability in intrinsic connectivity across some brain regions has been correlated with developmental state and the maturity of circuits (Dosenbach et al. 2010; Fair et al. 2008; Supekar et al. 2009;

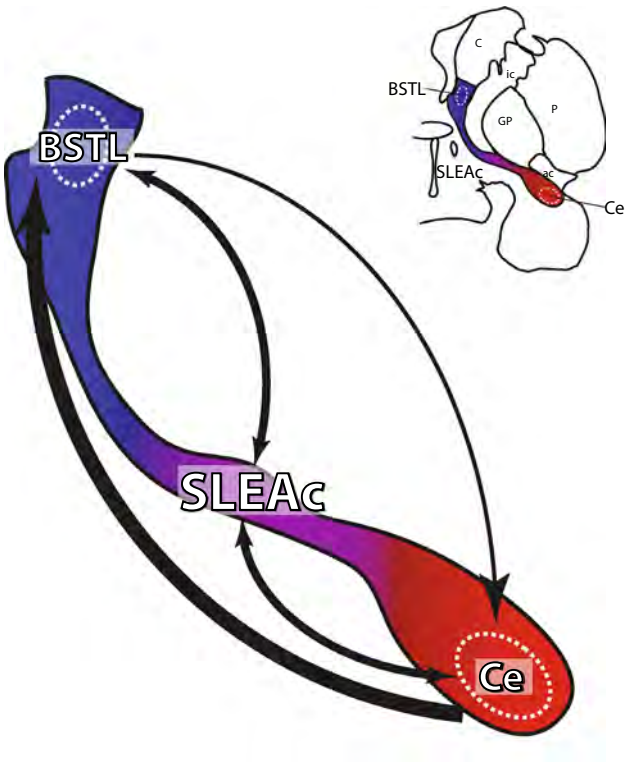

Fig. 8 Overview of the intrinsic connections of the EAc. Direct long connections favor the Ce → BSTL direction over the BSTL → Ce path. However, the dense reciprocal innervation of the SLEAc, by both the BSTL and Ce, reveals a substrate for recurrent connections and underscores the SLEAc's potential importance as a communication hub for extended amygdala information processing

Uddin et al. 2010; Vergun et al. 2013). While structural connections (as measured with deterministic tractography) between BST and Ce appear relatively stable over this early developmental time period, intrinsic connectivity between dorsal amygdala Ce region and the BST region was significantly greater at 7 weeks than at 3 weeks of age (Fig. 7b). Taken together, the imaging data confirm that the white matter pathways of the EAc are demonstrable early in the life of a primate, and indicate that functional integration of this circuit continues during postnatal development.

Implications for functional studies in humans and monkeys

The present findings indicate that, in primates, direct inputs from the Ce to BST dominate over the reverse pathway, and that functional coupling of the Ce and the BST is developing during infancy. The relative directionality of projections suggests that conditioned stimuli that drive behavioral responses via Ce also have strong, direct access to the BSTL, with the potential to influence BST-dependent responses over time. Consistent with their similar anatomic features and structural interconnectivitiy, the BSTL and Ce play related, but not identical, roles in mediating threat-related responses (Lee and Davis 1997; Walker and Davis 1997). In rodents, the Ce, but not BST, is required for the expression of short-lived, conditioned fear responses (Davis and Whalen 2001). In contrast, the BST, but not Ce, seems to be critical for threat-responses that are prolonged (Davis et al. 2010). In addition, there are dissociations between the Ce and BST in relation to threat conditioning, such that the Ce mediates discrete cue-related fear responses, whereas the BST is involved in mediating fear responses elicited by broader contexts (Alvarez et al. 2011; Fendt et al. 2003; Pego et al. 2008; Walker and Davis 2008; Zimmerman and Maren 2011). Evidence from rats and monkeys displaying anxiety-like behaviors (Duvarci et al. 2009; Fox et al. 2008; Jennings et al. 2013; Kalin et al. 2005; Kim et al. 2013), as well as from humans (Alvarez et al. 2011; Boll et al. 2013; Hasler et al. 2007; LaBar et al. 1998; Mobbs et al. 2010; Somerville et al. 2010, 2013; Straube et al. 2007), supports the idea that regions of the EAc are involved in maintaining threat-preparedness and initiating physiological and behavioral responses to threat.

The time course that we document for increased intrinsic coupling between the Ce and BST is similar to that for the development of young monkeys' abilities to regulate their capacity to respond to threat with context-appropriate behaviors (Kalin et al. 1991). More specifically, context-appropriate freezing behavior in response to the threat of a human intruder begins to occur around 2-months of age (Kalin et al. 1991), and we hypothesize that these new found abilities for regulating the fear response may result from the concomitant maturation of the EAc. Abundant and complex intrinsic synaptic connections among the Ce, BSTL, and SLEAc are likely being shaped between 3 and 7 weeks of age, and the associated developmental processes of synaptogenesis and synaptic pruning may be the source of neuronal change reflected in the maturation of Ce-BST functional connectivity. Future studies of the perinatal development of this system in a larger sample, and the influence of early-life stress on its structural and functional development, will be informative with respect to the ontogeny of adaptive and maladaptive fear and anxiety responses. The present study highlights the potential importance of the primate SLEAc for understanding EAc function in relation to adaptive and maladaptive anxiety. These data provide new insights into the biology and ontogenesis of the EAc, and build a foundation for understanding how the coordinated function of the EAc contributes to stress-related psychopathology.

Acknowledgments We gratefully acknowledge the technical expertise of Ms. Nanette Alcock and thank the personnel of the Harlow Center for Biological Psychology, the HealthEmotions

Research Institute, the Waisman Laboratory for Brain Imaging and Behavior, and the Wisconsin National Primate Research Center (WNPRC). This research was conducted in part at a facility constructed with support from Research Facilities Improvement Program Grant numbers RR15459-01 and RR020141-01. This work was supported by Grants from the National Institutes of Health: P51OD011106 (WNPRC); R01-MH063291 (JLF); F30-MH096502 (DMD); R01-MH046729 (NHK); R01-MH081884 (NHK); P50-MH100031 (RJD, NHK); T32 NS007-489-09 (LMC) and T32-MH018931-25. The content is solely the responsibility of the authors and does not necessarily represent the official views of the National Institutes of Health.

Compliance with ethical standards

Conflict of interest Dr. Kalin has received honoraria from CME Outfitters, Elsevier, and the Pritzker Neuropsychiatric Disorders Research Consortium. He is on the Advisory Boards for Corcept Therapeutics and Skyland Trail-George West Mental Health Foundation. Dr. Kalin is a Stockholder in Corcept Therapeutics, and owns several patents including: promoter sequences for corticotropin-releasing factor alpha (U.S. Patent #7071323, issued on 07-04-06); a method of identifying agents that alter the activity of the promoter sequences (U.S. Patent #7531356 issued on 05-12-09); promoter sequences for urocortin II and the use thereof (U.S. Patent #7087385 issued on 08-08-06); and promoter sequences for corticotropin-releasing factor binding protein and use thereof (U.S. Patent #7122650, issued on 10-17-06). All other authors declare no conflicts of interest.

References

Aggleton JP, Mishkin M (1984) Projections of the amygdala to the thalamus in the cynomolgus monkey. J Comp Neurol 222:56–68

Alheid GF, Heimer L (1988) New perspectives in basal forebrain organization of special relevance for neuropsychiatric disorders: the striatopallidal, amygdaloid, and corticopetal components of substantia innominata. Neuroscience 27:1–39

Alvarez RP, Chen G, Bodurka J, Kaplan R, Grillon C (2011) Phasic and sustained fear in humans elicits distinct patterns of brain activity. Neuroimage 55:389–400. doi:10.1016/j.neuroimage.2010.11.057

Amaral DG, Price JL, Pitkänen A, Carmichael ST (1992) Anatomical organization of the primate amygdaloid complex. In: Aggelton JP (ed) The amygdala: neurobiological aspects of emotion, memory, and mental dysfunction. Wiley-Liss, New York, pp 1–66

Avery SN, Clauss JA, Winder DG, Woodward N, Heckers S, Blackford JU (2014) BNST neurocircuitry in humans. Neuroimage 91:311–323. doi:10.1016/j.neuroimage.2014.01.017

Basser PJ, Pajevic S, Pierpaoli C, Duda J, Aldroubi A (2000) In vivo fiber tractography using DT-MRI data. Magn Reson Med 44:625–632

Bienkowski MS, Rinaman L (2013) Common and distinct neural inputs to the medial central nucleus of the amygdala and anterior ventrolateral bed nucleus of stria terminalis in rats. Brain Struct Funct 218:187–208. doi:10.1007/s00429-012-0393-6

Bienkowski MS, Wendel ES, Rinaman L (2013) Organization of multisynaptic circuits within and between the medial and the central extended amygdala. J Comp Neurol 521:3406–3431. doi:10.1002/cne.23356

Birn RM et al (2014) Evolutionarily conserved prefrontal-amygdalar dysfunction in early-life anxiety. Mol Psychiatry 19:915–922. doi:10.1038/mp.2014.46

Boll S, Gamer M, Gluth S, Finsterbusch J, Buchel C (2013) Separate amygdala subregions signal surprise and predictiveness during associative fear learning in humans. Eur J Neurosci 37:758–767. doi:10.1111/ejn.12094

Bunney BS, Aghajanian GK (1976) The precise localization of nigral afferents in the rat as determined by a retrograde tracing technique. Brain Res 117:423–435

Bupesh M, Abellan A, Medina L (2011) Genetic and experimental evidence supports the continuum of the central extended amygdala and a mutiple embryonic origin of its principal neurons. J Comp Neurol 519:3507–3531. doi:10.1002/cne.22719

Carpenter MB, Carlton SC, Keller JT, Conte P (1981) Connections of the subthalamic nucleus in the monkey. Brain Res 224:1–29

Cassell MD, Freedman LJ, Shi C (1999) The intrinsic organization of the central extended amygdala. Ann N Y Acad Sci 877:217–241

Chang LC, Jones DK, Pierpaoli C (2005) RESTORE: robust estimation of tensors by outlier rejection. Magn Reson Med 53:1088–1095. doi:10.1002/mrm.20426

Cho YT, Ernst M, Fudge JL (2013) Cortico-amygdala-striatal circuits are organized as hierarchical subsystems through the primate amygdala. J Neurosci 33:14017–14030. doi:10.1523/JNEUROSCI.0170-13.2013

Cook PA, Bai Y, Nedjati-Gilani S, Seunarine KK, Hall MG, Parker GJ, Alexander DC (2006) Camino: open-source diffusion-MRI reconstruction and processing. In: 14th scientific meeting of the international society for magnetic resonance in medicine, Seattle, p 2759

Cox RW (1996) AFNI: software for analysis and visualization of functional magnetic resonance neuroimages. Comput Biomed Res 29:162–173

Davis M, Whalen P (2001) The amygdala: vigilance and emotion. Mol Psychiatry 6:13–34

Davis M, Walker DL, Miles L, Grillon C (2010) Phasic vs sustained fear in rats and humans: role of the extended amygdala in fear vs anxiety. Neuropsychopharmacology 35:105–135. doi:10.1038/npp.2009.109

de Olmos JS (1990) Amygdala. In: Paxinos G (ed) The human nervous system. Academic Press, San Diego, pp 583–710

de Olmos J (2004) The Amygdala. In: Paxinos G, Mai JK (eds) The human nervous system, 2nd edn. Elsevier Academic Press, San Diego

de Olmos JS, Ingram WR (1972) The projection field of the stria terminalis in the rat brain. J Comp Neurol 146:303–333

deCampo DM, Fudge JL (2013) Amygdala projections to the lateral bed nucleus of the stria terminalis in the macaque: comparison with ventral striatal afferents. J Comp Neurol 521:3191–3216. doi:10.1002/cne.23340

Dong HW, Swanson LW (2004a) Organization of axonal projections from the anterolateral area of the bed nuclei of the stria terminalis. J Comp Neurol 468:277–298. doi:10.1002/cne.10949

Dong HW, Swanson LW (2004b) Projections from bed nuclei of the stria terminalis, posterior division: implications for cerebral hemisphere regulation of defensive and reproductive behaviors [erratum appears in J Comp Neurol. 2004 Jul 5;474(4):603–604]. J Comp Neurol 471:396–433

Dong HW, Petrovich GD, Swanson LW (2001a) Topography of projections from amygdala to bed nuclei of the stria terminalis. Brain Res Brain Res Rev 38:192–246

Dong HW, Petrovich GD, Watts AG, Swanson LW (2001b) Basic organization of projections from the oval and fusiform nuclei of the bed nuclei of the stria terminalis in adult rat brain. J Comp Neurol 436:430–455

Dosenbach NU et al (2010) Prediction of individual brain maturity using fMRI. Science 329:1358–1361. doi:10.1126/science.1194144

Duvarci S, Bauer EP, Pare D (2009) The bed nucleus of the stria terminalis mediates inter-individual variations in anxiety and fear. J Neurosci 29:10357–10361. doi:10.1523/JNEUROSCI.2119-09.2009

Fair DA et al (2008) The maturing architecture of the brain's default network. Proc Natl Acad Sci USA 105:4028–4032. doi:10.1073/pnas.0800376105

Fallon JH, Loughlin SE (1987) Monoamine innervation of cerebral cortex and a theory of the role of monoamines in cerebral cortex and basal ganglia. In: Jones EG, Peters A (eds) Cerebral cortex. Plenum Press, New York, pp 41–109

Fendt M, Endres T, Apfelbach R (2003) Temporary inactivation of the bed nucleus of the stria terminalis but not of the amygdala blocks freezing induced by trimethylthiazoline, a component of fox feces. J Neurosci 23:23–28

Fox AS, Kalin NH (2014) A translational neuroscience approach to understanding the development of social anxiety disorder and its pathophysiology. Am J Psychiatry. doi:10.1176/appi.ajp.2014.14040449

Fox AS, Shelton SE, Oakes TR, Davidson RJ, Kalin NH (2008) Trait-like brain activity during adolescence predicts anxious temperament in primates. PLoS ONE 3:e2570. doi:10.1371/journal.pone.0002570

Fox AS, Oler JA, Tromp DPM, Fudge JL, Kalin NH (2015) Extending the amygdala in theories of threat processing. Trends Neurosci **(in Press)**

Freedman LJ, Shi C (2001) Monoaminergic innervation of the macaque extended amygdala. Neuroscience 104:1067–1084

Freedman LJ, Insel TR, Smith Y (2000) Subcortical projections of area 25 (subgenual cortex) of the macaque monkey. J Comp Neurol 421:172–188

Freese JL, Amaral DG (2009) Neuroanatomy of the primate amygdala. In: Whalen PJ, Phelps EA (eds) The human amygdala. Guilford, NY, pp 3–42

Fudge JL, Haber SN (2000) The central nucleus of the amygdala projection to dopamine subpopulations in primates. Neuroscience 97:479–494

Fudge JL, Haber SN (2001) Bed nucleus of the stria terminalis and extended amygdala inputs to dopamine subpopulations in primates. Neuroscience 104:807–827

Fudge JL, Tucker T (2009) Amygdala projections to central amygdaloid nucleus subdivisions and transition zones in the primate. Neuroscience 159:819–841. doi:10.1016/j.neuroscience.2009.01.013

Fudge JL, Kunishio K, Walsh P, Richard C, Haber SN (2002) Amygdaloid projections to ventromedial striatal subterritories in the primate. Neuroscience 110:257–275

Fudge JL, Breitbart MA, McClain C (2004) Amygdaloid inputs define a caudal component of the ventral striatum in primates. J Comp Neurol 476:330–347

Fudge JL, deCampo DM, Becoats KT (2012) Revisiting the hippocampal-amygdala pathway in primates: association with immature-appearing neurons. Neuroscience 212:104–119. doi:10.1016/j.neuroscience.2012.03.040

Gaspar P, Berger B, Lesur A, Borsotti JP, Febvret A (1987) Somatostatin 28 and neuropeptide Y innervation in the septal area and related cortical and subcortical structures of the human brain. Distribution, relationships and evidence for differential coexistence. Neuroscience 22:49–73

Ghashghaei HT, Barbas H (2001) Neural interaction between the basal forebrain and functionally distinct prefrontal cortices in the rhesus monkey. Neuroscience 103:593–614

Gray TS, Magnuson DJ (1987) Neuropeptide neuronal efferents from the bed nucleus of the stria terminalis and central amygdaloid nucleus to the dorsal vagal complex in the rat. J Comp Neurol 262:365–374

Gray TS, Magnuson DJ (1992) Peptide immunoreactive neurons in the amygdala and the bed nucleus of the stria terminalis project to the midbrain central gray in the rat. Peptides 13:451–460

Grove EA (1988a) Efferent connections of the substantia innominata in the rat. J Comp Neurol 277:347–364

Grove EA (1988b) Neural associations of the substantia innominata in the rat: afferent connections. J Comp Neurol 277:315–346

Haber SN, Lynd E, Klein C, Groenewegen HJ (1990) Topographic organization of the ventral striatal efferent projections in the rhesus monkey: an anterograde tracing study. J Comp Neurol 293:282–298

Haber SN, Fudge JL, McFarland N (2000) Striatonigrostriatal pathways in primates form an ascending spiral from the shell to the dorsolateral striatum. J Neurosci 20(6):2369–2382

Halperin JJ, LaVail JH (1975) A study of the dynamics of retrograde transport and accumulation of horseradish peroxidase in injured neurons. Brain Res 100:253–269

Hasler G, Fromm S, Alvarez RP, Luckenbaugh DA, Drevets WC, Grillon C (2007) Cerebral blood flow in immediate and sustained anxiety. J Neurosci 27:6313–6319

Heimer L, Van Hoesen GW (2006) The limbic lobe and its output channels: implications for emotional functions and adaptive behavior. Neurosci Biobehav Rev 30:126–147. doi:10.1016/j.neubiorev.2005.06.006

Heimer L, de Olmos J, Alheid GF, Zaborszky L (1991) "Perestroika" in the basal forebrain: opening the border between neurology and psychiatry. Prog Brain Res 87:109–165

Heimer L, Harlan RE, Alheid GF, Garcia MM, de Olmos J (1997) Substantia innominata: a notion which impedes clinical-anatomical correlations in neuropsychiatric disorders. Neuroscience 76:957–1006

Heimer L et al (1999) The human basal forebrain. Part II. In: Bloom FE, Bjorkland A, Hokfelt T (eds) Handbook of chemical neuroanatomy, vol 15: the primate nervous system, part III. Elsevier, Amsterdam, pp 57–226

Huang H et al (2009) Anatomical characterization of human fetal brain development with diffusion tensor magnetic resonance imaging. J Neurosci 29:4263–4273. doi:10.1523/JNEUROSCI.2769-08.2009

Jennings JH, Sparta DR, Stamatakis AM, Ung RL, Pleil KE, Kash TL, Stuber GD (2013) Distinct extended amygdala circuits for divergent motivational states. Nature 496:224–228. doi:10.1038/nature12041

Jo HJ, Saad ZS, Simmons WK, Milbury LA, Cox RW (2010) Mapping sources of correlation in resting state FMRI, with artifact detection and removal. Neuroimage 52:571–582. doi:10.1016/j.neuroimage.2010.04.246

Johnston JB (1923) Further contributions to the study of the evolution of the forebrain. J Comp Neurol 35:337–481

Kalin NH, Shelton SE, Takahashi LK (1991) Defensive behaviors in infant rhesus monkeys: ontogeny and context-dependent selective expression. Child Dev 62:1175–1183

Kalin NH, Shelton SE, Fox AS, Oakes TR, Davidson RJ (2005) Brain regions associated with the expression and contextual regulation of anxiety in primates. Biol Psychiatry 58:796–804

Kaufmann WA, Barnas U, Maier J, Saria A, Alheid GF, Marksteiner J (1997) Neurochemical compartments in the human forebrain: evidence for a high density of secretoneurin-like immunoreactivity in the extended amygdala. Synapse 26:114–130

Kim SY et al (2013) Diverging neural pathways assemble a behavioural state from separable features in anxiety. Nature 496:219–223. doi:10.1038/nature12018

Klingler J, Gloor P (1960) The connections of the amygdala and of the anterior temporal cortex in the human brain. J Comp Neurol 115:333–369

Krüger O, Shiozawa T, Kreifelts B, Scheffler K, Ethofer T (2015) Three distinct fiber pathways of the bed nucleus of the stria terminalis to the amygdala and prefrontal cortex. Cortex 66:60–68. doi:10.1016/j.cortex.2015.02.007

LaBar KS, Gatenby JC, Gore JC, LeDoux JE, Phelps EA (1998) Human amygdala activation during conditioned fear acquisition and extinction: a mixed-trial fMRI study. Neuron 20:937–945

Lazar M et al (2003) White matter tractography using diffusion tensor deflection. Hum Brain Mapp 18:306–321. doi:10.1002/hbm.10102

Lee Y, Davis M (1997) Role of the hippocampus, the bed nucleus of the stria terminalis, and the amygdala in the excitatory effect of corticotropin-releasing hormone on the acoustic startle reflex. J Neurosci 17:6434–6446

Lesur A, Gaspar P, Alvarez C, Berger B (1989) Chemoanatomic compartments in the human bed nucleus of the stria terminalis. Neuroscience 32(1):181–194

Martin LJ, Powers RE, Dellovade TL, Price DL (1991) The bed nucleus-amygdala continuum in human and monkey. J Comp Neurol 309:445–485

McDonald AJ (2003) Is there an amygdala and how far does it extend? An anatomical perspective. Ann N Y Acad Sci 985:1–21

McDonald AJ, Shammah-Lagnado SJ, Shi C, Davis M (1999) Cortical afferents to the extended amygdala. Ann N Y Acad Sci 877:309–338

Miyashita T, Ichinohe N, Rockland KS (2007) Differential modes of termination of amygdalothalamic and amygdalocortical projections in the monkey. J Comp Neurol 502:309–324. doi:10.1002/cne.21304

Mobbs D, Yu R, Rowe JB, Eich H, FeldmanHall O, Dalgleish T (2010) Neural activity associated with monitoring the oscillating threat value of a tarantula. Proc Natl Acad Sci USA 107:20582–20586. doi:10.1073/pnas.1009076107

Moga MM, Herbert H, Hurley KM, Yasui Y, Gray TS, Saper CB (1990) Organization of cortical, basal forebrain, and hypothalamic afferents to the parabrachial nucleus in the rat. J Comp Neurol 295:624–661

Mori S, Aggarwal M (2014) In vivo magnetic resonance imaging of the human limbic white matter. Front Aging Neurosci 6:321. doi:10.3389/fnagi.2014.00321

Nagy FZ, Pare D (2008) Timing of impulses from the central amygdala and bed nucleus of the stria terminalis to the brain stem. J Neurophysiol 100:3429–3436. doi:10.1152/jn.90936.2008

Nance DM, Burns J (1990) Fluorescent dextrans as sensitive anterograde neuroanatomical tracers: applications and pitfalls. Brain Res Bull 25:139–145

Nauta WJ (1961) Fibre degeneration following lesions of the amygdaloid complex in the monkey. J Anat 95:515–531

Novotny GE (1977) A direct ventral connection between the bed nucleus of the stria terminalis and the amygdaloid complex in the monkey (*Macaca fascicularis*). J Hirnforsch 18:271–284

Oler JA et al (2012) Evidence for coordinated functional activity within the extended amygdala of non-human and human primates. Neuroimage 61:1059–1066. doi:10.1016/j.neuroimage.2012.03.045

Paxinos G, Huang X, Petrides M, Toga A (2009) The rhesus monkey brain in stereotaxic coordinates, 2nd edn. Academic Press, San Diego

Pego JM, Morgado P, Pinto LG, Cerqueira JJ, Almeida OF, Sousa N (2008) Dissociation of the morphological correlates of stress-induced anxiety and fear. Eur J Neurosci 27:1503–1516

Porrino LJ, Crane AM, Goldman-Rakic PS (1981) Direct and indirect pathways from the amygdala to the frontal lobe in rhesus monkeys. J Comp Neurol 198:121–136

Price JL, Amaral DG (1981) An autoradiographic study of the projections of the central nucleus of the monkey amygdala. J Neurosci 1:1242–1259

Pritchard TC, Hamilton RB, Norgren R (2000) Projections of the parabrachial nucleus in the old world monkey. Exp Neurol 165:101–117

Reynolds SM, Zahm DS (2005) Specificity in the projections of prefrontal and insular cortex to ventral striatopallidum and the extended amygdala. J Neurosci 25:11757–11767

Rinaman L, Levitt P, Card JP (2000) Progressive postnatal assembly of limbic-autonomic circuits revealed by central transneuronal transport of pseudorabies virus. J Neurosci 20:2731–2741

Rizvi TA, Ennis M, Behbehani MM, Shipley MT (1991) Connections between the central nucleus of the amygdala and the midbrain periaqueductal gray: topography and reciprocity. J Comp Neurol 303:121–131

Roberts GW (1992) Neuropeptides: celluler morphology, major pathways, and functional considerations. In: Aggelton JP (ed) The amygdala: neurobiological aspects of emotion, memory, and mental dysfunction. Wiley-Liss, New York, pp 115–142

Rose J, Vassar R, Cahill-Rowley K, Guzman XS, Stevenson DK, Barnea-Goraly N (2014) Brain microstructural development at near-term age in very-low-birth-weight preterm infants: an atlas-based diffusion imaging study. Neuroimage 86:244–256. doi:10.1016/j.neuroimage.2013.09.053

Rosene DL, Roy NJ, Davis BJ (1986) A cryoprotection method that facilitates cutting frozen sections of whole monkey brains for histological and histochemical processing without freezing artifact. J Histochem Cytochem 34(10):1301–1315

Russchen FT, Amaral DG, Price JL (1987) The afferent input to the magnocellular division of the mediodorsal thalamic nucleus in the monkey, *Macaca fascicularis*. J Comp Neurol 256:175–210

Schmued L, Kyriakidis K, Heimer L (1990) In vivo anterograde and retrograde axonal transport of the fluorescent rhodamine-dextran-amine, Fluoro-Ruby, within the CNS. Brain Res 526:127–134

Somerville LH, Whalen PJ, Kelley WM (2010) Human bed nucleus of the stria terminalis indexes hypervigilant threat monitoring. Biol Psychiatry 68:416–424. doi:10.1016/j.biopsych.2010.04.002

Somerville LH, Wagner DD, Wig GS, Moran JM, Whalen PJ, Kelley WM (2013) Interactions between transient and sustained neural signals support the generation and regulation of anxious emotion. Cereb Cortex 23:49–60. doi:10.1093/Cercor/Bhr373

Stefanacci L, Amaral DG (2002) Some observations on cortical inputs to the macaque monkey amygdala: an anterograde tracing study. J Comp Neurol 451:301–323

Straube T, Mentzel HJ, Miltner WH (2007) Waiting for spiders: brain activation during anticipatory anxiety in spider phobics. Neuroimage 37:1427–1436. doi:10.1016/j.neuroimage.2007.06.023

Sun N, Roberts L, Cassell MD (1991) Rat central amygdaloid nucleus projections to the bed nucleus of the stria terminalis. Brain Res Bull 27:651–662

Supekar K, Musen M, Menon V (2009) Development of large-scale functional brain networks in children. PLoS Biol 7:e1000157. doi:10.1371/journal.pbio.1000157

Swanson LW (2003) The amygdala and its place in the cerebral hemisphere. Ann N Y Acad Sci 985:174–184

Swanson LW, Petrovich GD (1998) What is the amygdala? Trends Neurosci 21:323–331

Torrisi S et al (2015) Resting state connectivity of the bed nucleus of the stria terminalis at ultra-high field. Hum Brain Mapp. doi:10.1002/hbm.22899

Turner BH, Zimmer J (1984) The architecture and some of the interconnections of the rat's amygdala and lateral periallocortex. J Comp Neurol 227:540–557

Uddin LQ, Supekar K, Menon V (2010) Typical and atypical development of functional human brain networks: insights from resting-state FMRI. Front Syst Neurosci 4:21. doi:10.3389/fnsys.2010.00021

Vasung L, Huang H, Jovanov-Milosevic N, Pletikos M, Mori S, Kostovic I (2010) Development of axonal pathways in the human fetal fronto-limbic brain: histochemical characterization and diffusion tensor imaging. J Anat 217:400–417. doi:10.1111/j.1469-7580.2010.01260.x

Veraart J et al (2011) Population-averaged diffusion tensor imaging atlas of the Sprague Dawley rat brain. Neuroimage 58:975–983. doi:10.1016/j.neuroimage.2011.06.063

Vercelli A, Repici M, Garbossa D, Grimaldi A (2000) Recent techniques for tracing pathways in the central nervous system of developing and adult mammals. Brain Res Bull 51:11–28

Vergun S et al (2013) Characterizing functional connectivity differences in aging adults using machine learning on resting state fMRI data. Front Comput Neurosci 7:38. doi:10.3389/fncom.2013.00038

Vincent JL et al (2007) Intrinsic functional architecture in the anaesthetized monkey brain. Nature 447:83–86. doi:10.1038/nature05758

Walker DL, Davis M (1997) Double dissociation between the involvement of the bed nucleus of the stria terminalis and the central nucleus of the amygdala in startle increases produced by conditioned versus unconditioned fear. J Neurosci 17:9375–9383

Walker DL, Davis M (2008) Role of the extended amygdala in short-duration versus sustained fear: a tribute to Dr. Lennart Heimer. Brain Struct Funct 213:29–42. doi:10.1007/s00429-008-0183-3

Wallace DM, Magnuson DJ, Gray TS (1992) Organization of amygdaloid projections to brainstem dopaminergic, noradrenergic, and adrenergic cell groups in the rat. Brain Res Bull 28:447–454

Walter A, Mai JK, Lanta L, Gorcs T (1991) Differential distribution of immunohistochemical markers in the bed nucleus of the stria terminalis in the human brain. J Chem Neuroanat 4:281–298

Wang R, Benner T, Sorensen AG, Wedeen VJ (2007) Diffusion toolkit: a software package for diffusion imaging data processing and tractography. In: Paper presented at the Proc. Intl. Soc. Mag. Reson. Med., Berlin, Germany, May 19th–25th

Woolrich MW et al (2009) Bayesian analysis of neuroimaging data in FSL. Neuroimage 45:S173–S186. doi:10.1016/j.neuroimage.2008.10.055

Yilmazer-Hanke DM (2012) Amygdala. In: Mai JK, Paxinos G (eds) The human nervous system. Academic Press, San Diego, pp 759–834

Zahm DS (2008) Accumbens in a functional-anatomical systems context. In: David H (ed) The nucleus accumbens: neurotransmitters and related behaviours. Transworld Research Network-Research Signpost, Kerala, pp 1–37

Zhang H, Yushkevich PA, Alexander DC, Gee JC (2006) Deformable registration of diffusion tensor MR images with explicit orientation optimization. Med Image Anal 10:764–785. doi:10.1016/j.media.2006.06.004

Zimmerman JM, Maren S (2011) The bed nucleus of the stria terminalis is required for the expression of contextual but not auditory freezing in rats with basolateral amygdala lesions. Neurobiol Learn Mem 95:199–205. doi:10.1016/j.nlm.2010.11.002